

Grain-Specific Transitions Determine the Band Edge Luminescence in Dion–Jacobson Type 2D Perovskites

Simon Kahmann,* Herman Duim, Alexander J. Rommens, Eelco K. Tekelenburg, Shuyan Shao, and Maria A. Loi*

The photophysics of 2D perovskites incorporating 1,4-phenylenedimethan-ammonium (PDMA) as spacer cations is studied. PDMA PbI_4 and PDMA SnI_4 exhibit absorption and luminescence spectra dominated by excitonic transitions and an emission due to two different states. Low-temperature studies reveal a time-dependent red shift of 12 meV that is correlated with grain-specific luminescence spectra observed in optical micrographs. For the Pb-variant, grains of red-shifted and lower intensity band edge emission simultaneously exhibit a more pronounced luminescence from a broad defect-related band around 2 eV. This suggests the grain-specific emission to be related to local defects. These observations have important consequences for the understanding of luminescence of 2D perovskites, for which peak splitting of the band edge emission is a common, yet not completely resolved observation.

metal halide octahedra. This opens a rich playing field for tuning the photophysical properties of these 2D compounds targeted to a variety of opto-electronic applications.^[1] Many studies have considered 2D compounds to increase the stability of 3D perovskites in solar cells and to facilitate charge extraction or to act as efficient emitters in light emitting devices.^[2,3]

The choice of the spacer cation can affect factors, such as moisture resistivity,^[4] or the degree of distortion in the inorganic slabs, which partially governs the band gap energy^[5] or the carrier effective masses.^[6] Recently, also the imposition of optical chirality^[7] or the mixing of states between spacers and inorganic moieties have become important topics of research.^[8]

1. Introduction

When compared to the tightly restricted choice of cations for 3D bulk perovskites, imposed by the Goldschmidt tolerance factor, layered 2D perovskites offer the opportunity to employ a plethora of different spacer cations to separate the inorganic

Traditionally, most of the organic spacers have been based on primary amines, such as the prototypical butylammonium (BA^+) or phenylethylammonium (PEA^+) giving rise to A_2MX_4 chemical formulas in so-called Ruddlesden–Popper (RP) compounds, where A is the spacer cation, M the metal cation, and X the halide anion.^[1] More recently, diammonium cations, forming AMX_4 Dion–Jacobson (DJ) structures, have moved into the spotlight of research.^[9,10] Instead of two spacer cations per unit cell, these compounds possess only one organic molecule with two functional groups to stabilize the layered structure. Although employed in solar cells and characterized for this purpose,^[11–13] fundamental studies on their photophysics are so far scarce.

The photophysics of 2D perovskites exhibits several intensively studied aspects. In particular, low-temperature studies reveal a rich substructure of the excitonic luminescence and absorption. High-energy features are commonly explained through exciton-phonon interactions. However, there is no consensus on the origin of the vibrational modes responsible for the observed spectral features and the actual mechanisms at play.^[14–16] Slightly Stokes-shifted band edge emission and split sub-peaks have been analyzed in the framework of dark and bright excitons,^[17,18] bright doublets,^[19] localized defects,^[16,20] and have been shown to depend on the angle of detection.^[20,21] At even lower energy, broad emission bands are sometimes attributed to self-trapped excitons, but have recently been proposed to be defect-related.^[22]


Here, we report on the photophysics of the prototypical compounds PDMA PbI_4 and PDMA SnI_4 , which are based on the

S. Kahmann, H. Duim, A. J. Rommens, E. K. Tekelenburg, S. Shao, M. A. Loi

Photophysics and OptoElectronics
Zernike Institute for Advanced Materials
University of Groningen
Nijenborgh 4, Groningen 9747 AG, The Netherlands
E-mail: sk2133@cam.ac.uk; m.a.loi@rugl.nl

S. Kahmann
Cavendish Laboratory
University of Cambridge
JJ Thomson Avenue, Cambridge CB30HE, UK

S. Shao
Institute of Molecular Aggregation Science
Tianjin University
Tianjin 300072, China

 The ORCID identification number(s) for the author(s) of this article can be found under <https://doi.org/10.1002/adom.202100892>.

© 2021 The Authors. Advanced Optical Materials published by Wiley-VCH GmbH. This is an open access article under the terms of the Creative Commons Attribution-NonCommercial-NoDerivs License, which permits use and distribution in any medium, provided the original work is properly cited, the use is non-commercial and no modifications or adaptations are made.

DOI: 10.1002/adom.202100892

dication 1,4-phenylenedimethan ammonium (PDMA^{2+}). Variation of the metal cation generates effects similar to RP structures, most prominently a band gap reduction for Sn-based compounds. The room temperature luminescence is formed by a convolution of two transitions and sample cooling brings their peak positions closer together.

When cooled with liquid helium, the band edge luminescence splits into two strong peaks, leading to a fast time-dependent red shift of 12 meV when monitoring the luminescence macroscopically. Both samples exhibit a large degree of photoluminescence (PL) heterogeneity, and by means of PL microscopy we can link the 12 meV shift to the presence of two distinct types of crystallites in the thin films: Type I crystallites exhibit an intense and blue-shifted band edge emission, whereas type II crystallites exhibit a red-shifted band edge emission and a larger contribution of a broad band at low energy. The broadband luminescence is due to defect-induced transitions, which consequently links the macroscopically observable peak-splitting to the presence of defect-related emission. This has important consequences for the understanding of band edge emission of 2D perovskites, as we expect this fundamental mechanism to play a similar role in related compounds.

2. Results

We fabricated thin films based on the prototypical diammonium dication, 1,4-phenylenedimethan ammonium (Figure 1a), which can be considered as the dicationic variant of

phenylmethylammonium (PMA), often used for RP type structures.^[5,23] In order to study the impact of metal variation on the photophysics, we employ either tin or lead to form PDMASnI_4 or PDMAPbI_4 , respectively. The spacer cation combines with the metal iodide octahedra, to form alternating layers, as stylized in Figure 1a. We confirm the layered structure from thin film X-ray diffraction (XRD) patterns in Figure 1b. The layer stacking predominantly occurs in the out-of-plane direction with respect to the substrate (layers run parallel to the surface), as indicated by the diffraction peaks at $2\theta = 14.3$, 21.5 , and 28.8° . Small contributions from planes stacked in in-plane directions can be identified by the diffraction peaks at 14.5 and 29.1° (consider Figure S1, Supporting Information).^[13]

Absorbance and PL in Figure 1c,d show spectra dominated by the excitonic behavior imposed by dielectric and quantum confinement of carriers into the inorganic slabs. Metal substitution shifts the excitonic peak energy toward the red spectral region when using Sn instead of Pb, as similarly observed for RP or 3D structures.^[16,24] In the current case, the absorbance of PDMAPbI_4 has a maximum around 2.41 eV, while that of the Sn-variant lies around 2.08 eV. The luminescence exhibits a relatively small Stokes shift in both cases (emission around 2.39 and 1.85 eV). Notably, both compounds exhibit an increasing absorbance already below the excitonic peak, which we attribute to the presence of shallow defects (particularly pronounced for PDMASnI_4).

A close look at the PL reveals asymmetric spectra that seem to be the convolution of two separate peaks. Variation of the incident laser power highlights this aspect: A shoulder around

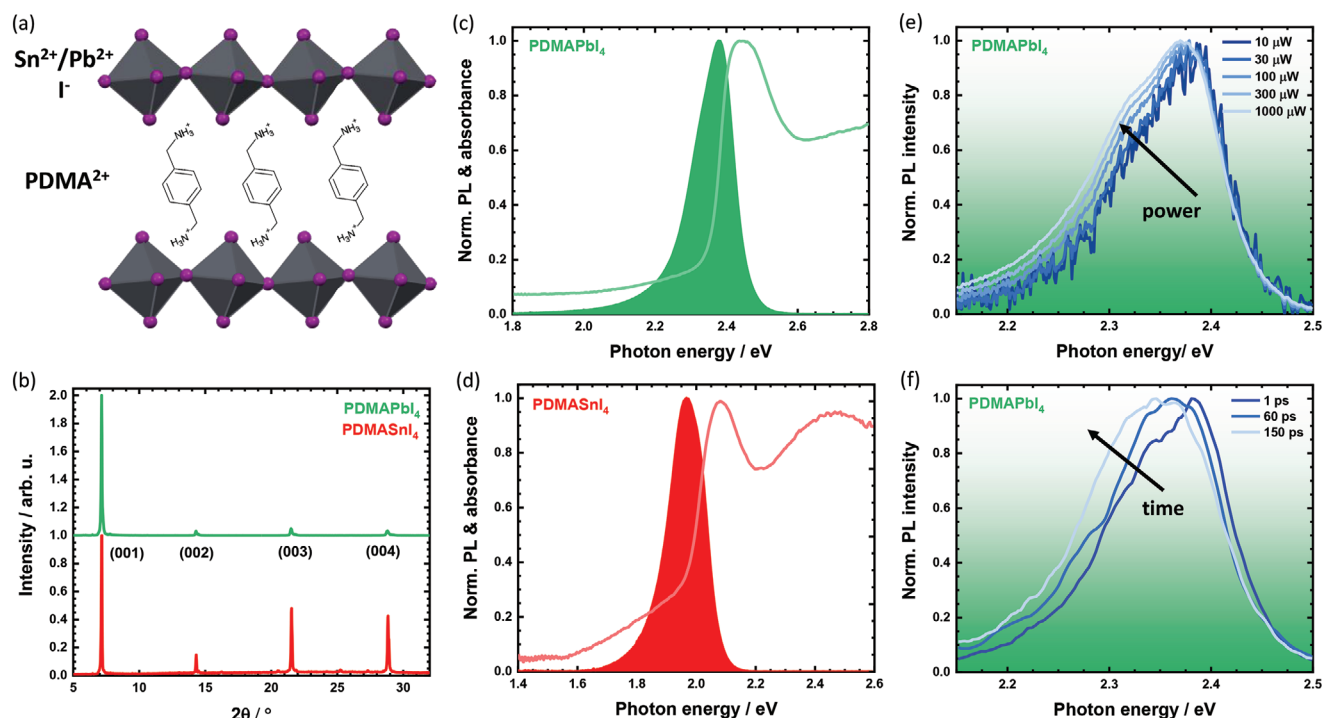


Figure 1. Sketch of the layered structure of inorganic slabs separated by organic spacer cations (a). The XRD spectra show a strong preferred stacking in out-of-plane direction, as indicated by the indexed (00n) peaks (b). Steady-state PL and absorbance spectra of PDMAPbI_4 (c) and PDMASnI_4 (d) highlight the excitonic transitions accompanied by a small Stokes shift. The PL is asymmetric in both cases and power-dependent (e), as well as time-dependent spectra (f) for the Pb-based variant highlight the presence of a shoulder around 2.3 eV additional to the main peak at 2.4 eV.

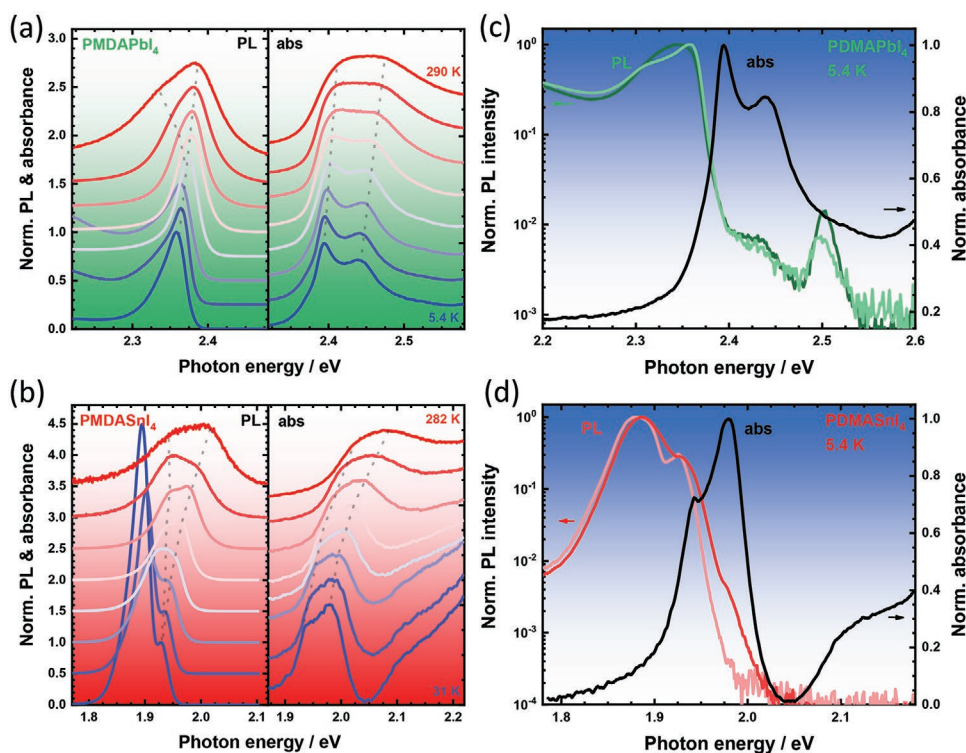


Figure 2. PL and absorbance spectra of PDMAPbI₄ (a) and PDMAStI₄ (b) for selected temperatures. The PL was normalized to the high-energy peak. Dotted lines guide the approximate shift of the peaks. Comparison of the absorbance and PL at 5.4 K for PDMAPbI₄ (c) and PDMAStI₄ (d). In both cases, two PL spectra highlight the sample heterogeneity.

2.33 eV for PDMAPbI₄ increases relatively for higher light intensity (Figure 1e). PDMAStI₄ shows an analogue behavior: A shoulder at the high-energy side of the emission decreases in relative intensity (2.01 vs. 1.97 eV; Figure S2, Supporting Information). In addition to the dependence on the excitation power, extended illumination also affects the shape of the spectrum and the relative contribution of the sub-peaks, as illustrated for PDMAStI₄ in Figure S3, Supporting Information.

Furthermore, when considering the transient PL at short delays, the emission undergoes a pronounced time-dependent red shift, shown for PDMAPbI₄ in Figure 1f (extracted transient PL in Figure S4, Supporting Information). The room temperature emission for both compounds is thus split into two contributions, of which the high-energy contribution emits more rapidly, which could be due to the relaxation toward a lower state.

In order to study the behavior more thoroughly and to elucidate the origin of the two peaks, we tracked the temperature-dependent absorption and PL when cooling the samples. **Figure 2** shows the steady-state data for the Pb-based sample in (a) and for the Sn-based variant in (b).

Temperature reduction shifts the main emission of PDMAPbI₄ to slightly lower energy from 2.39 to 2.36 eV, as indicated by the dotted line in Figure 2a. The overall band edge luminescence narrows, as expected from the suppression of thermal broadening, but it remains broad when compared to similar compounds based on primary amines.^[14,16,19] While the absorbance spectra follow this general trend, cooling also allows for a clear distinction of two peaks at 2.39 and 2.44 eV at

5.4 K. Notably, the low energy shoulder of the PL seems to blue shift at lower temperature—also consider the absolute intensity in Figure S5, Supporting Information.

PDMAStI₄ behaves similarly. Temperature reduction suppresses the thermal broadening of both the absorbance and the PL to clearly reveal two distinct peaks in the latter case. Simultaneously, the two shoulders observed in the room temperature luminescence move closer together, as observed above for PDMAPbI₄ and similarly reported for Ruddlesden–Popper compounds.^[25] Following similar observations for RP structures based on PEA⁺, the temperature-dependent spectral shifts of PDMAStI₄ are more pronounced than for the Pb-based compound.^[16] For example, the energy of the higher PL peak decreases from 2.01 to 1.93 eV over the temperature range (approx. 80 vs. 30 meV; Sn vs. Pb).

In contrast to PDMAPbI₄, the Sn-based variant develops an additional distinctly resolvable emission at lower energy that becomes increasingly strong when cooled. As underlined by the absolute PL spectra in Figure S5, Supporting Information, this low-energy peak not only grows relative to the upper one, but it increases the overall PL intensity of the compound at low temperature. This aspect is furthermore highlighted in Figure S6, Supporting Information: Cooling the samples down to 150 K exponentially increases the intensity for both compounds, but whereas the PDMAPbI₄ emission slightly decreases below this temperature, the trend continues monotonically for PDMAStI₄. In consequence, PDMAStI₄ follows the same trends as PDMAPbI₄, with the additional presence of a pronounced second emission peak around the band edge. Given

the energetic coincidence with the onset of the absorbance tail, we propose that this transition involves the shallow defects mentioned above, likely by promoting radiative recombination of bound excitons. Cooling suppresses phonon-mediated decay channels for these states. We note that the presence of such a pronounced second emission peak in Sn-based 2D perovskite structures seems to be a general observation.^[16,26,27] At the same time, we would like to note that the limited intensity increase of PDMAPbI₄ at low temperature is also related to a further broad emission band at significantly lower energy, typical for lead-based 2D perovskites, as discussed further below. Additional data on the dynamics of the PL can be found in Figures S7 to S9, Supporting Information.

In order to better understand the emission properties of the two compounds, it is expedient to consider the luminescence in context of the absorbance. At a first glance, the double-peak structure of the room temperature PL could be interpreted as a mirror image of the absorption (Franck–Condon series), which exhibits two shoulders at room temperature that become distinct peaks upon cooling. However, as we discussed above, the two PL sub-peaks move closer together upon initial cooling and become hardly resolvable at lower temperature, whereas the absorbance peaks remain separated over the entire temperature range. As we discuss below, the high-energy absorbance peak generates only weak PL that is not resolvable on a linear scale. In other words, the two PL sub-peaks at room temperature are not a mirror image of the absorbance.

Figure 2c,d shows the PL on a semi-logarithmic scale, which reveals additional weak peaks at high-energy. PDMAPbI₄

exhibits a pronounced emission at 2.50 eV and a broader signal around 2.43 eV. Both coincide with features in the absorbance, namely, the upper distinct absorbance peak at 2.43 eV and an inflection around 2.51 eV. For PDMAStI₄, a similar shoulder forms around 1.98 eV, slightly Stokes shifted from the upper pronounced absorbance peak.

These high-energy features are generally attributed to hot excitons, which recombine radiatively before complete relaxation to the lowest vibrational level of the excited state.^[14,16] Interestingly, the emission of the higher hot peak of PDMAPbI₄ is significantly stronger than the one found at 2.43 eV. Such an inversion of the expected behavior has so far not been reported for similar systems and could be due to increased reabsorption, given the overlap of the lower hot peak with areas of strong absorption. The obtained spacing amounts to approximately 70 meV for PDMAPbI₄ and 50 meV for PDMAStI₄ and thereby fall into a similar region as found previously for compounds based on primary amines.^[14–16] The situation here is inverted when compared with PEA₂PbI₄ and PEA₂StI₄. Those compounds exhibit a larger spacing for the Sn-based variant, adding further information to the so far unresolved mechanism. We note, however, that caution has to be taken in case of PDMAPbI₄, as trace amounts of PbI₂ could also give rise to PL at 2.50 eV.^[28]

When considering the time-resolved PL at low temperature shortly after excitation, given in Figure 3, the streak camera images in (a) and (d) show the emission from PDMAPbI₄ to be dominated by a single strong peak, whereas two distinct peaks are present for PDMAStI₄. Within the resolution of our

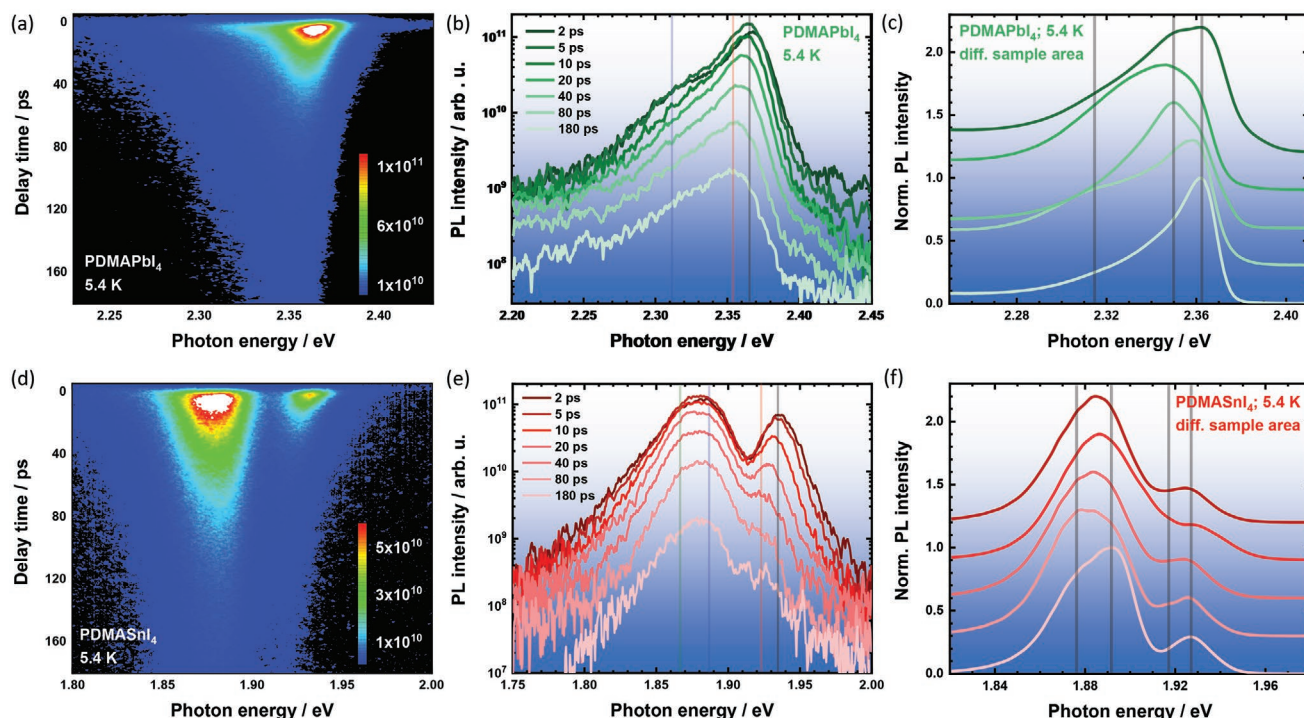


Figure 3. Time-resolved PL at 5.4 K and short delay time for PDMAPbI₄ (top row) and PDMAStI₄ (bottom). The streak images highlight the presence of two pronounced emission peaks of the tin-variant as opposed to the single peak of the lead-variant (a,d). Spectra at selected delays underline the red shift of high-energy emission (b,e). The PL spectra exhibit a large point-to-point variation that reveals several sub-peaks to form the dominant emission bands (c,f). Spectra in (c) and (d) were vertically offset for clarity.

set-up in the used configuration (≈ 4 ps), the onset dynamics of these two peaks are identical (Figure S10, Supporting Information). Although there is no distinct second luminescence peak observable for PDMAPbI₄ in this region, the main peak is clearly asymmetric with a pronounced tail towards low energy. The spectra, particularly at an early stage, show the presence of a broadened emission around 2.31 eV (indicated by a vertical line in Figure 3), which seems related to the more pronounced lower peak of the Sn-based variant.

As highlighted by the spectra in Figure 3b,e, the PL of the Pb-based compound exhibits a rapid initial red shift, similarly observed for the high-energy emission for the tin compound (indicated by vertical lines used to extract the transients). In both cases, this shift amounts to approximately 12 meV: from 2.366 to 2.354 eV for PDMAPbI₄ and from 1.934 to 1.922 eV for PDMAStI₄. The red shift manifests as a faster initial decay of the high-energy side of the two peaks, as indicated by the extracted transients in Figure S10, Supporting Information. In contrast, the low-energy emission of PDMAStI₄ exhibits a virtually mono-exponential decay at such short delays.

The presence of this initial red shift relates to a hotly debated topic in the field, namely the substructure of the band edge exciton in these compounds. In particular, for PEA₂PbI₄ band edge excitons have been said to split into pairs of either a bright and a dark state^[17,18] or into two bright states.^[19] Luminescence substructure has furthermore been attributed to the contribution to localised states, such as bound excitons.^[16,29] At the same time, the temperature-dependent data from Figure 2 suggests that this high-energy peak might be a convolution of the two sub-peaks observable at elevated temperature.

At low temperature, variation of the probed area on the samples reveals a strongly heterogeneous PL, as can be seen from spectra taken on different spots in Figure 3c,f. PDMAStI₄ exhibits changes determined by the relative contribution of at least three different states. Their position is highlighted by the vertical lines. We find a close pair of narrow peaks at 2.362 and 2.350 eV and a broader shoulder centered around 2.315 eV. Comparison with the semi-logarithmic data in Figure 2c shows these changes only affect the Stokes-shifted emission from fully relaxed excitons. Incidentally, the separation of the two high-energy features precisely amounts to the 12 meV found for the time-resolved red shift found in Figure 3b.

PDMAStI₄ reveals a similar picture. The point-to-point variation changes the relative intensity around four sub-peaks without changing the overall separation into two main PL bands. The two contributions of the upper peak are not as clearly distinguishable as for PDMAPbI₄, but close inspection shows the presence of a smaller sub-peak around 1.917 eV in addition to the more pronounced emission at 1.927 eV. Again, this separation is close to the time-dependent red shift. Furthermore, although the time-dependent data in Figure 3e (or Figure S10, Supporting Information) do not reveal any spectral shifts of the lower main peak on this time scale, the point-to-point variation shows the contribution of two distinct sub-peaks at 1.877 and 1.891 eV.

Photoluminescence microscopy helps to shed further light on the origin of the strong heterogeneity of the obtained spectra. The widefield micrograph in Figure S11, Supporting

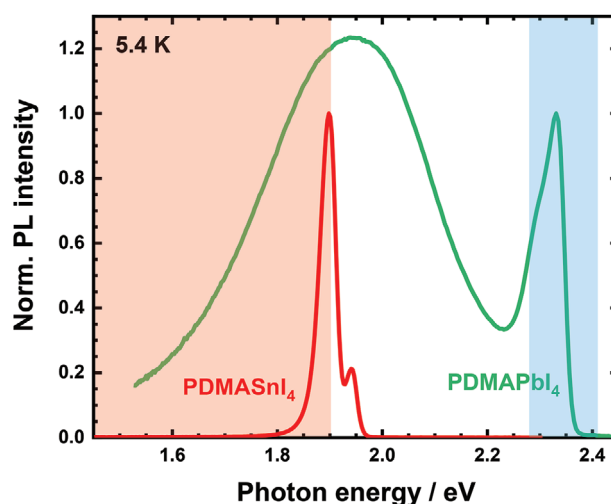


Figure 4. Overview PL spectra of PDMAPbI₄ and PDMAStI₄ at 5.4 K. Additional to the narrow emission peak of the band edge luminescence, the lead-based variant exhibits a broad and red-shifted band around 1.95 eV due to defect-mediated emission. PDMAStI₄ shows no such luminescence. The colored rectangles indicate the CLSM detection channels.

Information, shows the luminescence of PDMAPbI₄ at 4.3 K and reveals clear differences in colour and hue that seem to correlate with different crystallites. Therefore, we used confocal laser scanning microscopy (CLSM) to locally probe the luminescence and detected it through two channels: around the main emission peak (blue channel; 2.27–2.56 eV) as well as around a low energy band attributed the recombination via trap states, shown in Figure 4 (red channel; <1.91 eV).^[22] The corresponding maps are given in Figure 5a,b.

The blue channel PL map confirms the presence of micrometre-scale crystallites, some of which appear almost uniform in intensity (type I) and a second type of crystallites (type II) that exhibits a fine pattern of brighter intensity. The red channel, in contrast, reveals no such substructure and is largely dominated by two different areas of high and low intensity. Dark areas generally correspond to type I crystallites and bright areas to those of type II. The intensity ratio of the two channels, given in Figure 5c, highlights the correlation of the uniform areas in (a) with the dark areas in (b), seen by the intense blue colour in the false color plot.

Excluding the intricate substructure of type II crystallites, which will be subject to a follow-up study, there are thus at least two distinct sample regions that differ in their PL properties. The differences can be further quantified when taking the PL spectra locally for representative crystallites. Figure 5d shows the steady-state PL taken in three different locations for each type of crystallite, as indicated in Figure 5b. Although both types exhibit the dominant narrow peak around 2.37 eV and the trap-related emission, there are distinct differences between them.

First, as expected from the CLSM maps, type II crystallites exhibit a consistently higher PL intensity of the low energy band that has a maximum around 1.96 eV. This band is furthermore red-shifted with respect to type I crystallites, whose emission centres around 2.02 eV. As this band is attributed to defect-induced recombination, this suggests the presence of more than one type of defect. Conversely, the main peak intensity of

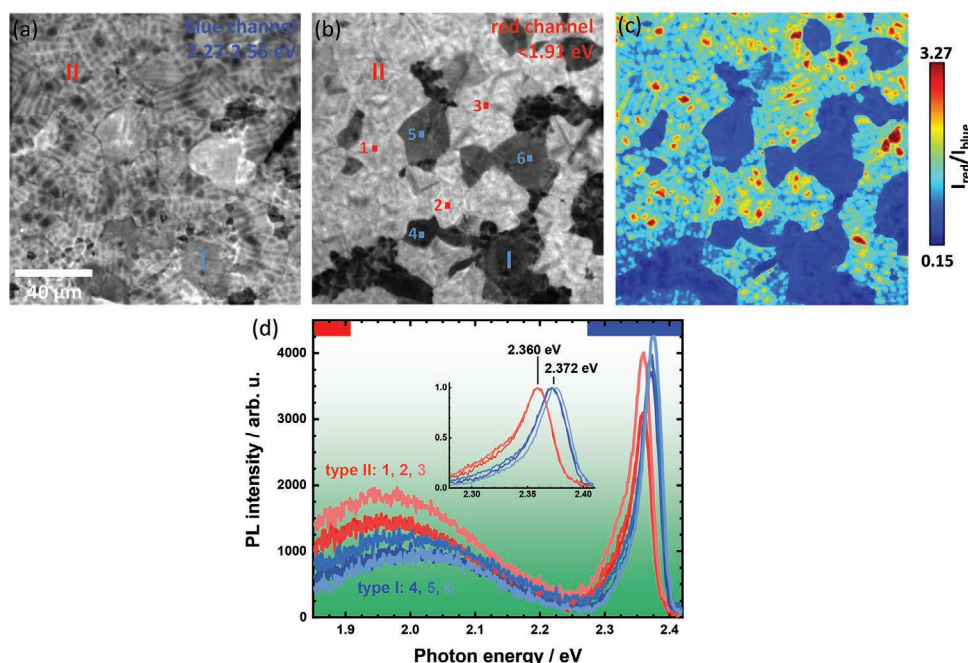


Figure 5. CLSM maps of PDMAPI₄ at 4.3 K. The PL was mapped around the main peak (a) and the low energy band (b). Taking the intensity ratio of the channels highlights the presence of at least two different types of crystallites (c). Extracted steady-state spectra for selected points (indicated in (b)), although largely similar, reveal a red shift of 12 meV in areas of more pronounced low energy emission (d).

type I crystallites is higher and, more importantly, close inspection of the normalized spectra in the inset reveals the peak position to be shifted by 12 meV for the two areas. Thus, crystallites that exhibit a stronger low energy emission (type II) also possess a red-shifted band edge luminescence.

Thin films of PDMAPI₄ exhibit an even larger heterogeneity of the PL in CLSM maps, as shown in Figure S12, Supporting Information. However, the material also exhibits a much stronger morphological heterogeneity, rendering its analysis more complex. Therefore, in the following discussion, we focus on the observations for PDMAPI₄, noting that PDMAPI₄ similarly shows strong peak shifts and intensity variations for different crystal grains.

3. Discussion

The PL maps in Figure 5 and Figure S12, Supporting Information, suggest the large-scale PL heterogeneity is linked to spectral variations between different crystal grains. Although a grain-specific trapping site that affects the intensity of band edge luminescence was previously observed for PEA₂PbI₄,^[30] grain-to-grain spectral variations have so far not been reported. The agreement between the two peak positions with the time-dependent red shift of Figure 3 acquired macroscopically suggests that these effects share a common origin. The clear correlation between the red-shifted main peak and the more pronounced broad emission at 2 eV for PDMAPI₄ further suggests that the reduced energy of the main peak could also be related to the presence of defects.^[22]

The nature of the band edge emission in these layered compounds is currently hotly debated. Reports on the more widely

studied Ruddlesden–Popper type perovskites usually refer to the presence of three brightly emitting states,^[16–19] of which the upper two strongly resemble the two subpeaks we observe in the current Dion–Jacobson compound. Traditionally, the two subpeaks were explained through an intrinsic splitting of the band edge exciton into an upper bright and a lower dark state,^[17,18] and more recently through a pair of differently polarized bright states.^[19] In contrast, we recently found strong evidence for the lower state to be due to a localised state and proposed it was linked to defects.^[16] The latter proposition agrees well with our current findings on the Dion–Jacobson compounds.

It is important to highlight that previous works claiming the action of localised states were based on techniques probing large-scale areas and the effect of carrier localization was inferred from the magnetic field-dependent behavior or the effect of varied excitation intensity.^[16,28,29] Here, however, PL mapping allows us to link the two peaks to distinct crystal grains that not only differ with respect to the position of the main peak, but also in terms of the defect-related emission at low energy (Figure 4). Assuming an identical origin of the peak splitting in the two families of compounds, the current study further suggests an extrinsic origin.

The observation of the peak splitting also in single crystals (of PEA₂PbI₄)^[18,19] can be explained by the intensity of the two peaks being governed by the concentration of defects. This is supported by the presence of the broad emission around 2 eV that is also present in type II grains. It is surprising, though, to observe two types of grains with such a stark contrast instead of a more continuous behaviour.

At the same time, we note that evidence has been brought forward for different crystallite orientations in the DJ thin films, which could give rise to the observed properties. It was recently

reported that, although predominantly forming crystallites with out-of-plane stacking direction (relative to the substrate), thin films of PDMA PbI_4 can exhibit a non-negligible amount of in-plane stacked crystallites.^[13] This insight was acquired through X-ray diffraction based on the presence of additional peaks at $2\theta = 14.5^\circ$ and 29.1° . However, our diffraction data, shown in Figure 1d, exhibit only minor contributions at these angles (also consider Figure S1, Supporting Information). This contrast likely stems from the different fabrication protocol, as we promoted the crystal growth via the use of an anti-solvent that was omitted in prior studies (see experimental part). Given the ubiquity of the two different crystallites, this small amount of in-plane oriented crystals seems to be an unlikely origin for the PL heterogeneity. Nonetheless, several studies reported spectral variation upon out-of-plane PL detection for 2D perovskites, in which low energy peaks are typically more pronounced.^[20,21,31] An orientation-dependent PL spectrum is not necessarily mutually exclusive with defect-related emission around the band edge: inter-plane excitons at grain boundaries have, for example, been invoked to explain the orientational behaviour.^[20] Furthermore, defect formation energies might be facet dependent, leading to spectral changes when viewing crystallites from different directions.

Finally, we would like to note that during the finalization of this manuscript Kaiser et al. published a study that also reported on low-temperature PL data of PDMA PbI_4 .^[32] The authors observed similar spectral features including the recombination of free, localized, and bound excitons, as well as a broad emission band, which, however, they attribute to surface PbI_2 rather than PDMA PbI_4 itself. Importantly, their attribution of bound excitons on the low-energy side corresponds well with our interpretation of the pronounced peak of PDMA SnI_4 and the persistent shoulder observable for the lead-based variant. Nonetheless, the authors did not address sample heterogeneities and likely assigned their “localized exciton” to what we show are transitions from type II grains, thus highlighting the deeper insight obtained here by use of PL microscopy.

4. Conclusion

We studied the photoluminescence and absorbance of two different compounds of the Dion–Jacobson family of 2D perovskites. PDMA PbI_4 and PDMA SnI_4 exhibit room temperature luminescence composed of two convoluted transitions, which move closer together upon cooling. A large heterogeneity in the thin film PL can be attributed to grain-specific emission properties. For PDMA PbI_4 , the two different types of crystallites exhibit a 12 meV shift of the main emission peak, for which the red-shifted grains simultaneously exhibit a lower intensity and a stronger contribution from a low-energy band attributed to defects. The peak energy separation corresponds to a time-dependent red shift of the macroscopic luminescence at short delay times that was similarly observed for the more commonly studied Ruddlesden–Popper compounds. The current PL heterogeneity has thus important consequences for the broader understanding of luminescence properties in the field of 2D perovskites, and future work will have to address a possible

connection between these variations in grain-specific luminescence and differences in crystallite orientation.

5. Experimental Section

Synthesis: Thin films of PDMA PbI_4 and PDMA SnI_4 were deposited on quartz substrates for PL and absorption experiments and on glass for X-ray diffraction. Precursor solutions for both perovskites were obtained through dissolving lead iodide/tin iodide and 1,4-phenylenedimethan ammonium diiodide (PDMA I_2) in a mixed solvent composed of *n,n*-dimethylformamide (DMF) and dimethyl sulfoxide (DMSO), at 4:1 volume ratio. In order to suppress the further oxidation of Sn^{2+} ions, a small amount of SnF_2 was added in the case of PDMA SnI_4 .

In a typical experiment, 156.8 mg PDMA I_2 were mixed with 148.8 mg SnI_2 and 6.3 mg SnF_2 in 0.4 mL DMF and 0.1 mL DMSO. Alternatively, 156.8 mg PDMA I_2 were mixed with 184.6 mg PbI_2 in 0.4 mL DMF and 0.1 mL DMSO.

Prior to deposition, the substrates were ultrasonically cleaned through a series of four baths of detergent solution, deionized water, acetone, and isopropanol—at each step, sonication occurred for two periods of 10 min, with the solvent being replaced after the first leg. Subsequently, the substrates were dried for 10 min at 140°C and subjected to an ultraviolet ozone treatment for 20 min before immediately being transferred into a nitrogen-filled glovebox for film deposition. The perovskite film was deposited using a single-step spin programme antisolvent method. The spinning speed was set to 5000 rpm with a duration of 50 s; the antisolvent (toluene) was applied perpendicular to the substrate 35 s into the spin programme. Upon completion, the films were immediately transferred to a hot plate to be annealed at 120°C for 20 min. The remaining solvent quickly evaporated upon heating leading to a rapid crystallization of the perovskite and color change to bright red/yellow for the tin and lead-based compound, respectively.

XRD: A Bruker D8 Advanced diffractometer operating in a Bragg–Brentano geometry equipped with a $\text{CuK}\alpha$ radiation source ($\lambda = 1.54 \text{ \AA}$) and a Lynxeye detector were used to measure the X-ray diffraction patterns of the thin films. All XRD measurements were performed under ambient conditions.

Absorption and PL Spectroscopy: All optical characterization was performed under inert atmosphere, without prior exposure of the sample to ambient conditions. The samples were mounted into a cryostat (Oxford Optistat CF) and excited at 3.1 eV (400 nm) using the second harmonic of a mode-locked Ti:sapphire laser (Mira 900, coherent) emitting at a repetition rate of 76 MHz. Steady-state spectra were recorded with a Hamamatsu EM-CCD camera that was spectrally calibrated. Employed gratings exhibit 150 lines mm^{-1} (50 for the overview spectra). The excitation beam was spatially limited by an iris and focused with a lens of 150 mm focal length. The fluence was adjusted using grey filters and the spectra were taken in reflection with an incident angle of approximately 30° with respect to the sample normal. Time-resolved traces were taken with a Hamamatsu streak camera working in synchroscan mode. Measurements occurred under helium atmosphere. Absorbance spectra were taken in the same set-up and by using a tungsten lamp as white light source with continuous spectrum. The transmission of a blank quartz substrate was taken as reference.

Confocal Laser Scanning Microscopy: CLSM images and widefield fluorescence micrographs were acquired with a Nikon CI confocal microscope system equipped with a CFI S Plan Fluor ELWD 40 \times objective. The widefield illumination occurred with the 436 nm line of a mercury lamp. For CLSM, samples were excited by a 488 nm continuous wave laser, and the photoluminescence was detected either by using a set of photomultiplier tubes equipped with optical filters ($515 \pm 30 \text{ nm}$ band pass or 650 nm long pass) or by directing the light with an optical filter into the beam path of the spectroscopy set-up described above. During the measurement, the samples were mounted with silver paste in an Oxford HiRes cryostat kept under vacuum.

Supporting Information

Supporting Information is available from the Wiley Online Library or from the author.

Acknowledgements

Arjen Kamp and Teodor Zaharia are thanked for technical support. S.K. is grateful for a research fellowship (Grant No: 408012143) awarded by the Deutsche Forschungsgemeinschaft (DFG). E.K.T. acknowledges the financial support of the Zernike Institute of Advanced Materials. This work was financed through the Materials for Sustainability (Mat4Sus) programme (739.017.005) of the Netherlands Organisation for Scientific Research (NWO). This work is part of the research program of the Foundation for Fundamental Research on Matter (FOM), which is part of the Netherlands Organization for Scientific Research (NWO). This is a publication of the FOM focus Group "Next Generation Organic Photovoltaics" participating in the Dutch Institute for Fundamental Energy Research (DIFFER).

Conflict of Interest

The authors declare no conflict of interest.

Data Availability Statement

The data that support the findings of this study are available from the corresponding author upon reasonable request.

Keywords

confocal microscopy, defects, Dion–Jacobson, excitons, metal halide perovskites, photoluminescence

Received: May 5, 2021

Revised: August 9, 2021

Published online: September 12, 2021

- [1] J.-C. Blancon, J. Even, C. C. Stoumpos, M. G. Kanatzidis, A. D. Mohite, *Nat. Nanotechnol.* **2020**, *15*, 969.
- [2] G. Grancini, M. K. Nazeeruddin, *Nat. Rev. Mater.* **2019**, *4*, 4.
- [3] N. Wang, L. Cheng, R. Ge, S. Zhang, Y. Miao, W. Zou, C. Yi, Y. Sun, Y. Cao, R. Yang, Y. Wei, Q. Guo, Y. Ke, M. Yu, Y. Jin, Y. Liu, Q. Ding, D. Di, L. Yang, G. Xing, H. Tian, C. Jin, F. Gao, R. H. Friend, J. Wang, W. Huang, *Nat. Photonics* **2016**, *10*, 699.
- [4] J. Shi, Y. Gao, X. Gao, Y. Zhang, J. Zhang, X. Jing, M. Shao, *Adv. Mater.* **2019**, *31*, 1901673.
- [5] K.-Z. Du, Q. Tu, X. Zhang, Q. Han, J. Liu, S. Zauscher, D. B. Mitzi, *Inorg. Chem.* **2017**, *56*, 9291.
- [6] M. Baranowski, P. Plochocka, *Adv. Energy Mater.* **2020**, *10*, 1903659.
- [7] M. K. Jana, R. Song, H. Liu, D. R. Khanal, S. M. Janke, R. Zhao, C. Liu, Z. Vally Vardeny, V. Blum, D. B. Mitzi, *Nat. Commun.* **2020**, *11*, 4699.
- [8] J. Xue, R. Wang, X. Chen, C. Yao, X. Jin, K.-L. Wang, W. Huang, T. Huang, Y. Zhao, Y. Zhai, D. Meng, S. Tan, R. Liu, Z.-K. Wang, C. Zhu, K. Zhu, M. C. Beard, Y. Yan, Y. Yang, *Science* **2021**, *371*, 636.
- [9] L. Mao, W. Ke, L. Pedesseau, Y. Wu, C. Katan, J. Even, M. R. Wasielewski, C. C. Stoumpos, M. G. Kanatzidis, *J. Am. Chem. Soc.* **2018**, *140*, 3775.
- [10] M.-H. Tremblay, J. Bacsa, B. Zhao, F. Pulvirenti, S. Barlow, S. R. Marder, *Chem. Mater.* **2019**, *31*, 6145.
- [11] Y. Li, J. V. Milić, A. Ummadisingu, J.-Y. Seo, J.-H. Im, H.-S. Kim, Y. Liu, M. I. Dar, S. M. Zakeeruddin, P. Wang, A. Hagfeldt, M. Grätzel, *Nano Lett.* **2019**, *19*, 150.
- [12] M. C. Gélvez-Rueda, P. Ahlwat, L. Merten, F. Jahanbakhshi, M. Mladenović, A. Hinderhofer, M. I. Dar, Y. Li, A. Dučinskis, B. Carlsen, W. Tress, A. Ummadisingu, S. M. Zakeeruddin, F. Schreiber, A. Hagfeldt, U. Rothlisberger, F. C. Grozema, J. V. Milić, M. Graetzel, *Adv. Funct. Mater.* **2020**, *30*, 2003428.
- [13] A. Dučinskis, G. Y. Kim, D. Moia, A. Senocrate, Y.-R. Wang, M. A. Hope, A. Mishra, D. J. Kubicki, M. Siczek, W. Bury, T. Schneeberger, L. Emsley, J. V. Milić, J. Maier, M. Grätzel, *ACS Energy Lett.* **2021**, *6*, 337.
- [14] D. B. Straus, S. Hurtado Parra, N. Iotov, J. Gebhardt, A. M. Rappe, J. E. Subotnik, J. M. Kikkawa, C. R. Kagan, *J. Am. Chem. Soc.* **2016**, *138*, 13798.
- [15] A. R. Srimath Kandada, C. Silva, *J. Phys. Chem. Lett.* **2020**, *11*, 3173.
- [16] S. Kahmann, H. Duim, H. H. Fang, M. Dyksik, S. Adjokatse, M. Rivera Medina, M. Pitaro, P. Plochocka, M. A. Loi, *Adv. Funct. Mater.* **2021**, <https://doi.org/10.1002/adfm.202103778>.
- [17] K. Tanaka, T. Takahashi, T. Kondo, K. Umeda, K. Ema, T. Umebayashi, K. Asai, K. Uchida, N. Miura, *Jpn. J. Appl. Phys.* **2005**, *44*, 5923.
- [18] H. H. Fang, J. Yang, S. Adjokatse, E. Tekelenburg, M. E. Kamminga, H. Duim, J. Ye, G. R. Blake, J. Even, M. A. Loi, *Adv. Funct. Mater.* **2020**, *30*, 1907979.
- [19] T. T. H. Do, A. Granados del Águila, D. Zhang, J. Xing, S. Liu, M. A. Prosnikov, W. Gao, K. Chang, P. C. M. Christianen, Q. Xiong, *Nano Lett.* **2020**, *20*, 5141.
- [20] M. Wang, J. Tang, H. Wang, C. Zhang, Y. S. Zhao, J. Yao, *Adv. Opt. Mater.* **2020**, *8*, 1901780.
- [21] R. A. DeCrescent, X. Du, R. M. Kennard, N. R. Venkatesan, C. J. Dahlman, M. L. Chabinyc, J. A. Schuller, *ACS Nano* **2020**, *14*, 8958.
- [22] S. Kahmann, E. K. Tekelenburg, H. Duim, M. E. Kamminga, M. A. Loi, *Nat. Commun.* **2020**, *11*, 2344.
- [23] M. E. Kamminga, H. H. Fang, M. R. Filip, F. Giustino, J. Baas, G. R. Blake, M. A. Loi, T. T. Palstra, *Chem. Mater.* **2016**, *28*, 4554.
- [24] A. Goyal, S. McKechnie, D. Pashov, W. Tumas, M. V. Schilfgaarde, V. Stevanović, *Chem. Mater.* **2018**, *30*, 3920.
- [25] R. A. DeCrescent, N. R. Venkatesan, C. J. Dahlman, R. M. Kennard, X. Zhang, W. Li, X. Du, M. L. Chabinyc, R. Zia, J. A. Schuller, *Sci. Adv.* **2020**, *6*, eaay4900.
- [26] V. V. Nawale, T. Sheikh, A. Nag, *J. Phys. Chem. C* **2020**, *124*, 21129.
- [27] G. Folpini, D. Cortecchia, A. Petrozza, A. R. Srimath Kandada, *J. Mater. Chem. C* **2020**, *8*, 10889.
- [28] E. K. Tekelenburg, S. Kahmann, M. E. Kamminga, G. R. Blake, M. A. Loi, *Adv. Opt. Mater.* **2021**, 2001647.
- [29] T. Neumann, S. Feldmann, P. Moser, J. Zerhoch, T. van de Goor, A. Delhomme, T. Winkler, J. J. Finley, C. Faugeras, M. S. Brandt, A. V. Stier, F. Deschler, *arXiv:2009.13867* **2020**.
- [30] H. Duim, S. Adjokatse, S. Kahmann, G. H. ten Brink, M. A. Loi, *Adv. Funct. Mater.* **2020**, *30*, 1907505.
- [31] T. Sheikh, A. Shinde, S. Mahamuni, A. Nag, *ACS Energy Lett.* **2018**, *3*, 2940.
- [32] M. Kaiser, Y. Li, J. Schwenzer, M. Jakoby, I. Allegro, M. Gerhard, M. Koch, A. Ducinskis, B. S. Richards, M. Graetzel, J. V. Milić, U. W. Paetzold, I. A. Howard, *J. Appl. Phys.* **2021**, *129*, 123101.